UCSD/PTH 00-25
MPI-PhT/2001-04
hep-ph/0102257

The Running Coulomb Potential and Lamb Shift in QCD

Andre H. Hoang*
Max-Planck-Institut für Physik
(Werner-Heisenberg-Institut)
Föhringer Ring 6, 80805 München, Germany

Aneesh V. Manohar†, Iain W. Stewart‡
Department of Physics, University of California at San Diego,
9500 Gilman Drive, La Jolla, CA 92093, USA

Abstract

The QCD β-function and the anomalous dimensions for the Coulomb potential and the static potential first differ at three loop order. We evaluate the three loop ultrasoft anomalous dimension for the Coulomb potential and give the complete three loop running. Using this result, we calculate the leading logarithmic Lamb shift for a heavy quark-antiquark bound state, which includes all contributions to the binding energies of the form $m\,\alpha_s^4(\alpha_s \ln \alpha_s)^k$, $k \geq 0$.

*ahoang@mppmu.mpg.de

†amanohar@ucsd.edu

‡iain@schwinger.ucsd.edu

I. INTRODUCTION

In this paper, we construct the three-loop anomalous dimension for the Coulomb potential in non-relativistic QCD (NRQCD) [1,2]. The formalism we use was developed in Refs. [3–6] and will be referred to as vNRQCD, an effective theory for heavy non-relativistic quark-antiquark pairs. Part of our computation is related to the running of the static potential [7], however effects associated with motion of the quarks do play an important role. Our final result for the Coulomb potential differs from the static potential at terms beyond those with a single logarithm (i.e. starting at four loops). Combining our Coulomb potential running with previous results for the running of the $1/m$ and $1/m^2$ potentials [4,6] allows us to compute the next-to-next-to-leading logarithmic (NNLL) corrections in the perturbative energy of a heavy $Q\bar{Q}$ bound state, which includes the sum of terms $m\,\alpha_s^4(\alpha_s \ln \alpha_s)^k$, $k \geq 0$, where m is the heavy quark pole mass. This contribution is the QCD analog of the QED $\alpha^5 \ln \alpha$ Lamb shift computed by Bethe. In QED, the series $m\,\alpha^4(\alpha \ln \alpha)^k$ terminates after the $k = 1$ term [8]. In QCD, there is an infinite series due to the running QCD coupling as well as the presence of non-trivial anomalous dimensions for other QCD operators. The results presented here also contribute to the NNLL prediction for the cross section for $e^+e^- \to t\bar{t}$ near threshold [9]. Implications for $b\bar{b}$ sum rules will be addressed in a future publication.

The expansion parameter of the effective theory is the quark velocity v. A quark has a momentum of order mv and an energy of order mv^2. We assume that m is large enough that $mv^2 \gg \Lambda_{\rm QCD}$ and a perturbative description of the bound state as a Coulombic system is valid. For a Coulombic bound state, α_s is of order v and contributions suppressed by both v and α_s are of the same order. It is useful to distinguish between powers of α_s and v when carrying out the matching and when evolving couplings and operators in the effective theory, and to only take $v \sim \alpha_s$ for the power counting of bound state matrix elements. In the effective theory, the quark-antiquark potentials appear as four-quark operators [2]. A potential of the form $\alpha_s^r/|\mathbf{k}|^s$ is of order $\alpha_s^r v^{1-s}$, where $\mathbf{k}$ is the fermion momentum transfer. With this power counting the time-ordered product of a v^a and v^b potential is of order v^{a+b}. Up to next-to-next-to-leading order (NNLO) the heavy quark potential has contributions

$$V \sim \left[\,\frac{\alpha_s}{v}\,\right] + \left[\,\frac{\alpha_s^2}{v}\,\right] + \left[\,\frac{\alpha_s^3}{v} + \alpha_s^2 v^0 + \alpha_s v\,\right] + \ldots . \tag{1}$$

The order $\alpha_s/v \sim 1$ term in Eq. (1) is the Coulomb potential generated at tree-level. The next-to-leading order (NLO) term is the one-loop correction to the Coulomb potential. The

NNLO terms are the two-loop correction to the Coulomb potential, the one-loop value for the $1/(m|\mathbf{k}|)$ potential, and the tree-level contribution to the order $|\mathbf{k}|^0/m^2$ potential. Writing the $Q\bar{Q}$ energy as $E = 2m + \Delta E$, the terms in Eq. (1) generate contributions of the following order in the binding energy:

$$\Delta E \sim \left[m\alpha_s^2\right] + \left[m\alpha_s^3\right] + \left[m\alpha_s^4\right] + \dots \,. \tag{2}$$

In Eqs. (1) and (2) the expansion has been performed at the scale $\mu = m$ so the coupling constants are $\alpha_s = \alpha_s(m)$. A typical perturbative expansion contains logarithms of μ divided by the various physical scales in the bound state. If the logarithms are large, fixed order perturbation theory breaks down, and one finds a large residual μ dependence. One can minimize the logarithms by setting μ to a value appropriate to the dynamics of the non-relativistic system. This is accomplished by summing large logarithms using the renormalization group, and using renormalization group improved perturbation theory. For $Q\bar{Q}$ bound states, the large logarithms are logarithms of $v \sim \alpha_s$, and can be summed using the velocity renormalization group (VRG) [3]. For the binding energy this gives the expansion

$$\begin{aligned} \Delta E &= \Delta E^{LL} + \Delta E^{NLL} + \Delta E^{NNLL} + \dots \,, \\ &\sim \left[m \sum_{k=0}^{\infty} \alpha_s^{k+2} (\ln \alpha_s)^k\right] + \left[m \sum_{k=0}^{\infty} \alpha_s^{k+3} (\ln \alpha_s)^k\right] + \left[m \sum_{k=0}^{\infty} \alpha_s^{k+4} (\ln \alpha_s)^k\right] + \dots \,, \end{aligned} \tag{3}$$

where the terms are the leading log (LL), next-to-leading log (NLL), and next-to-next-to-leading log (NNLL) results respectively.

In the VRG, one uses a subtraction velocity ν that is evolved from 1 to v. This simultaneously lowers the momentum cutoff scale $\mu_S = m\nu$ from m to mv and the energy cutoff scale $\mu_U = m\nu^2$ from m to mv^2. The VRG properly accounts for the coupling between energy and momentum caused by the equations of motion for the non-relativistic quarks. QED provides a highly non-trivial check of the VRG method. In Ref. [8] it was used to correctly reproduce terms in the subleading series of logarithms, including the $\alpha^3 \ln^2 \alpha$ corrections to the ortho and para-positronium decay rates, the $\alpha^7 \ln^2 \alpha$ hyperfine splittings for Hydrogen and positronium, and the $\alpha^8 \ln^3 \alpha$ Lamb shift for Hydrogen. The difference between the VRG, which involves the evolution of the momentum and the energy scale in a single step, and a conventional two stage renormalization group treatment, $m \to mv \to mv^2$, was examined in Ref. [10].

In section II we review the definition of potentials for non-static heavy quarks in the effective theory. In section III we compare these potentials with the Wilson loop definition

which is appropriate for static quarks. In section IV we rederive the leading-logarithmic (LL) and next-to-leading-logarithmic (NLL) results for the $Q\bar{Q}$ binding energy using the effective theory and discuss the two-loop matching for the Coulomb potential using the results in Refs. [11,12]. We also discuss some subtleties in the correspondence between diagrams in the static theory and soft diagrams in the effective theory. In section V we compute the three-loop anomalous dimension for the Wilson coefficient of the Coulomb potential. Results for the NNLL energy are given in section VI, followed by conclusions in section VII. In Appendix A we give some technical details on the structure of divergences in the effective theory, and in Appendix B we list some functions that appear in the energy at NNLL order.

II. THE VNRQCD POTENTIALS

The effective theory vNRQCD has soft gluons with coupling constant $\alpha_S(\nu)$, ultrasoft gluons with coupling constant $\alpha_U(\nu)$, as well as quark-antiquark potentials. The potential is the momentum dependent coefficient of a four-fermion operator:

$$\mathcal{L} = -\sum_{\mathbf{p},\mathbf{p}'} V(\mathbf{p},\mathbf{p}') \left[\psi_{\mathbf{p}'}{}^\dagger \psi_{\mathbf{p}} \chi_{-\mathbf{p}'}{}^\dagger \chi_{-\mathbf{p}}\right], \tag{4}$$

where spin and color indices are suppressed. The coefficient $V(\mathbf{p},\mathbf{p}')$ has an expansion in powers of v, $V = V_{(-1)} + V_{(0)} + V_{(1)} + \ldots$, where $V_{(-1)} = V_c$ is the Coulomb potential. For equal mass fermions

$$\begin{aligned}
V_c &= (T^A \otimes \bar{T}^A)\frac{\mathcal{V}_c^{(T)}}{\mathbf{k}^2} + (1\otimes 1)\frac{\mathcal{V}_c^{(1)}}{\mathbf{k}^2},\\
V_{(0)} &= (T^A \otimes \bar{T}^A)\frac{\pi^2\mathcal{V}_k^{(T)}}{m\,|\mathbf{k}|} + (1\otimes 1)\frac{\pi^2\mathcal{V}_k^{(1)}}{m\,|\mathbf{k}|},\\
V_{(1)} &= (T^A \otimes \bar{T}^A)\left[\frac{\mathcal{V}_2^{(T)}}{m^2} + \frac{\mathcal{V}_s^{(T)}\mathbf{S}^2}{m^2} + \frac{\mathcal{V}_r^{(T)}\,(\mathbf{p}^2+\mathbf{p}'^2)}{2\,m^2\,\mathbf{k}^2} - \frac{i\mathcal{V}_\Lambda^{(T)}\,\mathbf{S}\cdot(\mathbf{p}'\times\mathbf{p})}{m^2\mathbf{k}^2} + \frac{\mathcal{V}_t^{(T)}T(\mathbf{k})}{m^2}\right]\\
&\quad +(1\otimes 1)\left[\frac{\mathcal{V}_2^{(1)}}{m^2} + \frac{\mathcal{V}_s^{(1)}}{m^2}\,\mathbf{S}^2\right],
\end{aligned} \tag{5}$$

where $\mathbf{k} = \mathbf{p}' - \mathbf{p}$, $\mathbf{S} = (\boldsymbol{\sigma_1} + \boldsymbol{\sigma_2})/\mathbf{2}$, $T(\mathbf{k}) = (\delta^{ij} - 3\mathbf{k}^i\mathbf{k}^j/\mathbf{k}^2)\boldsymbol{\sigma}_1^i\boldsymbol{\sigma}_2^j$. The Wilson coefficients, $\mathcal{V}^{(T,1)}$ depend on the subtraction velocity ν. In Eq. (5) the color decomposition $V = (T^A\otimes\bar{T}^A)V^{(T)} + (1\otimes 1)V^{(1)}$ has been used and the potential in the color singlet channel is $V^{(s)} = V^{(1)} - C_F V^{(T)}$. (The Casimirs of the adjoint and fundamental representations are denoted by

C_A and C_F, respectively.) At LL order the running of the coefficients $\mathcal{V}_{2,s,r}^{(1,T)}$ was computed in Ref. [4] and $\mathcal{V}_{\Lambda,t}^{(1,T)}$ in Ref. [4,13], while the NLL order running of $\mathcal{V}_k^{(1,T)}$ was computed in Ref. [6]. In this work we compute the running of $\mathcal{V}_c^{(s)}$ at NNLL order. This allows the computation of the $Q\bar{Q}$ energy spectrum at NNLL order.

In vNRQCD additional potential-like effects are generated by loops with soft gluons, for which the Feynman rules can be found in Refs. [3,5]. Matrix elements of soft gluon diagrams contribute to the energy beginning at NLO. In contrast, matrix elements with ultrasoft gluons start at N^{3}LO. The renormalization group improved energies are obtained by computing the anomalous dimensions for these soft interactions and the four fermion operators in Eq. (5).

III. THE STATIC POTENTIAL VERSUS THE COULOMB POTENTIAL

Parts of our analysis are related to the study of the static limit of QCD which describes heavy quarks in the $m \to \infty$ limit. We therefore briefly review the pertinent results which have been derived in this framework.

In position space the static QCD potential is defined as the expectation value of the Wilson loop operator,

$$V_{\rm stat}(r) = \lim_{T\to\infty} \frac{1}{T} \ln \left\langle \mathrm{Tr}\, P \exp -ig \oint_C A_\mu dx^\mu \right\rangle , \tag{6}$$

where C is a rectangle of width T and fixed height r. This potential is independent of the mass m of the quarks and depends only on r. In QCD perturbation theory the static potential is known at two-loop order [11,12] . These calculations use static fermion sources with propagators which are identical to those in Heavy Quark Effective Theory [14]. The exponentiation of the static potential [15,16] guarantees that one can avoid dealing with graphs which have pinch singularities in momentum space. The analysis of Refs. [15,16] also gives a prescription for the color weight factors for different graphs based on the c-web theorem.

In Ref. [17], Appelquist, Dine and Muzinich (ADM) pointed out that at three loops the static potential in Eq. (6) has infrared (IR) divergences from graphs of the form in Fig. 1a,b. In the color singlet channel Fig. 1a has color factor $C_F C_A^2 (C_A - 2C_F)$ while Fig. 1b is proportional to $C_F^2 C_A^2$. Taking into account the exponentiation of $V_{\rm stat}$ using the c-web theorem, the color singlet contribution to $V_{\rm stat}$ from Fig. 1(a,b) is simply Fig. 1a with the

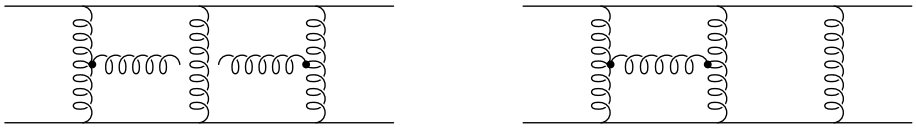

(a) (b)

FIG. 1. Graphs contributing to the three-loop IR divergence of the QCD static potential.

color factor replaced by $C_A^3 C_F$, and is IR divergent. ADM showed that this IR divergence could be avoided by summing a class of diagrams—those of Fig. 1 with the addition of an arbitrary number of gluon rungs. Summing over these diagrams regulates the IR divergence by building up Coulombic states for the static quark sources. The summation gives a factor $\exp\Big([V^{(s)}(r)-V^{(o)}(r)]T\Big)$ for the propagation of the intermediate color-octet $Q\bar{Q}$ pair, where $V^{(s)}(r)$ and $V^{(o)}(r)$ are the color-singlet and color-octet potentials. The exponential factor suppresses long-time propagation of the intermediate color-octet state, and regulates the IR divergence by introducing an IR cutoff scale of order $[V^{(s)}(r) - V^{(o)}(r)] \sim \alpha_s/r$.

In Ref. [18] the ADM divergence in the static potential was studied by Brambilla et al. using the effective theory pNRQCD [2]. They made the important observation that along with potential contributions, the definition in Eq. (6) contains contributions from ultrasoft gluons, and the latter are responsible for the ADM IR divergence. They showed that the ADM IR divergence in QCD matches with an IR divergence of a pNRQCD graph that describes the selfenergy of a quark-antiquark system due to an ultrasoft gluon with momenta $q^\mu \sim \alpha_s/r$. Therefore, the static potential in pNRQCD can be defined as a matching coefficient of a four fermion operator, as in Eq. (4), in an infrared safe manner. We will refer to this potential as the soft-static potential. The ultrasoft pNRQCD graph also has an ultraviolet divergence. Brambilla et al. computed the coefficient of this divergence and extracted a new $\ln(\mu)$ contribution to the soft-static potential. In Ref. [7] the three-loop anomalous dimension was computed for the soft-static potential in this framework. In the color singlet channel for scales $\mu \sim \alpha_s(r)/r$ their solution reads

$$V_{\rm stat}(\mu, r) = V_{\rm stat}^{(\rm 2loops)}(r) - \frac{1}{4\pi r}\left[\frac{2\pi C_F C_A^3}{3\beta_0}\alpha_s^3(r)\ln\left(\frac{\alpha_s(r)}{\alpha_s(\mu)}\right)\right], \tag{7}$$

where the first term is the two loop static potential derived in Refs. [11,12].

For large but finite m the effective theory for $Q\bar{Q}$ bound states has an expansion in v. The quark potential in this case differs from that in the static case, and in general one cannot obtain the static theory by taking the $m \to \infty$ limit. To illustrate this consider as

FIG. 2. Loop with an insertion of the $1/(m|\mathbf{k}|)$ and $1/\mathbf{k^2}$ potentials.

an example the loop graph involving the iteration of a $1/(m|\mathbf{k}|)$ and a Coulomb potential as shown in Fig. 2. In the effective theory for non-static fermions, the fermion propagators give a factor proportional to m. The final result for the graph is independent of m and is the same order in v as the Coulomb potential. On the other hand, if we first take the static limit $m \to \infty$, then $1/(m|\mathbf{k}|) \to 0$, and there is no such graph. This example illustrates the general result that the static theory is not obtained as the $m \to \infty$ (or $v \to 0$) limit of the non-static effective theory. Loop integrals can produce factors of m or $1/v$, and thereby cause mixing between operators which are of different orders[1] in v. Furthermore, the energy and the momentum transfer in Coulombic states are coupled by the quark equations of motion. We will see that for this reason the anomalous dimension of the static and Coulomb potentials differ at three loops. The three-loop matching for the static and Coulomb potentials can also differ.

IV. THE COULOMB POTENTIAL AT ONE AND TWO LOOPS

In this work dimensional regularization and the $\overline{\rm MS}$ scheme will be used. The $\overline{\rm MS}$ QCD running coupling constant will be denoted by $\overline{\alpha}_s(\mu)$, and is determined by the solution of the renormalization group equation

$$\begin{aligned}\mu\frac{{\rm d}\overline{\alpha}_s(\mu)}{{\rm d}\mu} &= \overline{\beta}\left(\overline{\alpha}_s(\mu)\right)\\ &= -2\beta_0\frac{\overline{\alpha}_s^2(\mu)}{4\pi} - 2\beta_1\frac{\overline{\alpha}_s^3(\mu)}{(4\pi)^2} - 2\beta_2\frac{\overline{\alpha}_s^4(\mu)}{(4\pi)^3} + \ldots\,. \end{aligned} \tag{8}$$

In a mass-independent subtraction scheme β_0 and β_1 are scheme-independent. The notation $\overline{\alpha}_s^{[n]}(\mu)$ will be used to indicate the solution of Eq. (8) with coefficients up to β_{n-1} (i.e. n loop order) kept in the β-function.

In the VRG, the soft and ultrasoft subtraction scales μ_S and μ_U are given by $\mu_S = m\nu$ and $\mu_U = m\nu^2$. We define the soft and ultrasoft anomalous dimensions γ_S and γ_U as the

[1]However, we stress that if powers of α_s are also counted as powers of v, then operators which are higher order in v never mix into lower order operators.

derivatives with respect to $\ln \mu_S$ and $\ln \mu_U$, respectively. The derivative with respect to $\ln \nu$ gives the total anomalous dimension, $\gamma = \gamma_S + 2\gamma_U$. vNRQCD has three independent but related coupling constants that are relevant for our calculation: the soft gluon coupling $\alpha_S(\nu)$, the ultrasoft gluon coupling $\alpha_U(\nu)$, and the coefficient of the Coulomb potential $\mathcal{V}_c(\nu)$. The tree-level matching conditions at $(\mu = m \Leftrightarrow \nu = 1)$ are

$$\alpha_S(1) = \alpha_U(1) = \overline{\alpha}_s(m)\,, \qquad \mathcal{V}_c^{(T)}(1) = 4\pi\overline{\alpha}_s(m)\,, \qquad \mathcal{V}_c^{(1)}(1) = 0\,, \tag{9}$$

and the solutions of the one-loop renormalization group equations for the coupling constants in the effective theory are [19,3]

$$\begin{aligned} \alpha_S\,(\nu) &= \overline{\alpha}_s^{[1]}(m\nu)\,, & \alpha_U\,(\nu) &= \overline{\alpha}_s^{[1]}(m\nu^2)\,, \\ \mathcal{V}_c^{(T)}(\nu) &= 4\pi\overline{\alpha}_s^{[1]}(m\nu)\,, & \mathcal{V}_c^{(1)}(\nu) &= 0. \end{aligned} \tag{10}$$

In deriving the above equations, it has been assumed that any light fermions have masses much smaller than mv^2, so that there are no mass thresholds in the renormalization group evolution. If there is a mass threshold larger than mv^2 and widely separated from mv and m, then it is possible to also include such effects in the effective theory, see Ref. [3].

At leading order the Hamiltonian for the color singlet $Q\bar{Q}$ system is

$$H_0 = \frac{\mathbf{p^2}}{m} + \frac{\mathcal{V}_c^{(s)}(\nu)}{\mathbf{k^2}}\,. \tag{11}$$

To minimize large logarithms in higher order matrix elements we run ν to the bound state velocity v_b, which we define as the solution of the equation

$$v_b = \frac{a_c(\nu = v_b)}{n} = \frac{C_F\,\overline{\alpha}_s^{[1]}(mv_b)}{n}\,, \tag{12}$$

where for convenience we have defined

$$a_c(\nu) = -\,\frac{\mathcal{V}_c^{(s)}(\nu)}{4\pi}\,, \tag{13}$$

and n is the principal quantum number. The LL binding energy is then simply the eigenvalue of the Schrödinger equation, $H_0|\psi_{n,l}\rangle = \Delta E|\psi_{n,l}\rangle$ with the LL solution for the Coulomb potential, $\mathcal{V}_c^{(s)}(\nu) = -C_F\mathcal{V}_c^{(T)}(\nu)$ from Eq. (10). Thus,

$$\Delta E^{LL} = -\frac{m}{4n^2}\,[a_c(\nu)]^2 \tag{14a}$$

$$= -\frac{m}{4\,n^2}\,C_F^2\left[\overline{\alpha}_s^{[1]}(mv_b)\right]^2 = -\frac{mv_b^2}{4}\,, \tag{14b}$$

where in the second line we have evaluated the energy at the low scale $\nu = v_b$. Higher order corrections to the energy are all evaluated as perturbative matrix elements with the leading order wavefunctions, $|\psi_{n,l}\rangle$.

Consider how the results in Eq. (10) are extended to higher orders. The graphs for the renormalization of the ultrasoft gluon self coupling have the same rules as for QCD, and those for the renormalization of the lowest order soft gluon vertex have the same rules as for HQET. Since the momenta of soft and ultrasoft gluons are cleanly separated there is no mixing of scales, so the anomalous dimension for α_S is independent of α_U and vica-versa. Thus, one expects that in the $\overline{\rm MS}$ scheme $\alpha_S(\nu) = \overline{\alpha}_s(m\nu)$ and $\alpha_U(\nu) = \overline{\alpha}_s(m\nu^2)$ to all orders.

However, the coefficient of the Coulomb potential can differ from $4\pi\overline{\alpha}_s(m\nu)$ at higher orders. At one-loop, the only order α_s^2/v graph in the effective theory is the soft diagram [5][2]

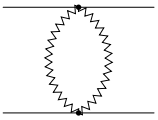

$$= \frac{-i\mu_S^{2\epsilon}\alpha_S^2(\nu)}{\mathbf{k^2}}(T^A \otimes \bar{T}^A)\left[\frac{\beta_0}{\epsilon} + \beta_0 \ln\left(\frac{\mu_S^2}{\mathbf{k^2}}\right) + a_1\right], \tag{15}$$

where $\beta_0 = 11/3C_A - 4T_F n_\ell/3$ and $a_1 = 31C_A/9 - 20T_F n_\ell/9$ in the $\overline{\rm MS}$ scheme, and n_ℓ is the number of light soft quarks. The divergence in Eq. (15) is canceled by a counterterm for $\mathcal{V}_c^{(T)}$, causing it to run with anomalous dimension $-2\beta_0\alpha_S^2(\nu)$. The remaining terms in the soft graph are identical to the one-loop soft-static potential calculation and also reproduce the set of $\alpha_s^2/\mathbf{k^2}$ terms in full QCD with dimensional regularization parameter μ. The one-loop matching correction to $\mathcal{V}_c^{(T,1)}(1)$ is the difference between the full and effective theory diagrams and therefore vanishes at the matching scale $\mu = \mu_S = m$.

A correspondence between the soft-static potential calculation and soft order $1/v$ diagrams is expected to persist at higher orders in α_s as well. The Feynman rules for the soft vertices are almost identical to the HQET rules used for soft-static potential calculations. There are a few notable differences. In the effective theory it is not necessary to use the exponentiation theorem [15,16] to eliminate diagrams with pinch singularities of the form

$$\int \mathrm{d}q^0 \, \frac{1}{(q0 + i\epsilon)(-q0 + i\epsilon)} \,. \tag{16}$$

These are automatically removed in the construction of the tree level soft vertices because the $1/q_0$ factors in the soft Feynman rules do not contain $i\epsilon$'s, and in evaluating diagrams

[2]Note that the soft loop includes soft gluons, soft light quarks, as well as soft ghosts.

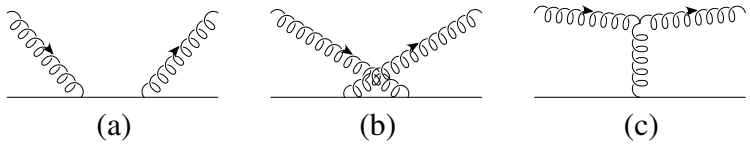

FIG. 3. Compton scattering graphs that contribute to the soft vertex.

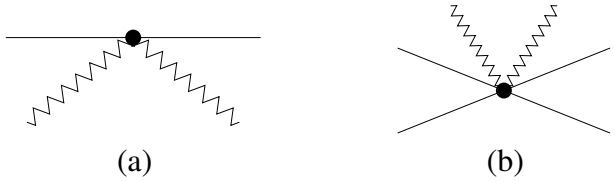

FIG. 4. Examples of vertices involving soft gluons.

these poles are ignored. For example [3], from matching the full theory Compton scattering graphs in Fig. 3 one obtains the soft vertex in Fig. 4a which is proportional to $[T^A, T^B]/q_0$, where terms proportional to $\{T^A, T^B\}$ have canceled. In the soft-static calculations this cancellation instead takes place at the level of the box and crossed box graphs, and is guaranteed by exponentiation. For the soft-static potential it is known that at higher orders there are contributions from the $i\pi\delta(q_0)$ terms that originate from the $i\epsilon$'s. It was exactly this type of contribution that was missed in the two-loop calculation by Peter [11], and was correctly identified by Schröder [12]. In the effective theory these delta function contributions belong to the potential regime [6], and soft-static graphs with this type of contribution are reproduced by operators such as the one shown in Fig. 4b, where a soft gluon scatters from a potential. Matching induces these operators to account for the difference between the full and effective theory graphs for Compton scattering off two quarks. Thus, the treatment of $i\epsilon$'s does affect the correspondence between soft-static and soft graphs. The total contribution of the graphs in the static theory with $k^\mu \sim mv$ gluons is reproduced in the effective theory by graphs with soft gluons.

A real difference between the soft-static and effective theory calculations is the way in which counterterms are implemented. The soft-static potential is defined by local HQET-like Feynman rules and all UV divergent contributions from soft gluons are absorbed into vertex, field, and coupling renormalization. The renormalization of the four point function is taken care of by the renormalization of the two and three point functions. Renormalization of the vNRQCD diagrams is quite different because potential gluons are not treated as degrees of freedom. The effective theory has graphs with soft gluons and in addition the four-quark

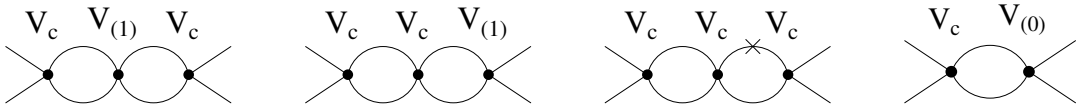

FIG. 5. Order α_s^3/v diagrams with potential iterations. The $\times$ denotes an insertion of the $\mathbf{p^4}/8m^3$ relativistic correction to the kinetic term.

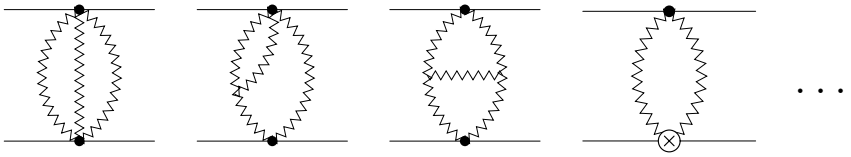

FIG. 6. Examples of order α_s^3/v diagrams with soft vertices. The vertex with a cross denotes an insertion of a one-loop counterterm.

Coulomb potential operator. The overall divergence in soft graphs, such as the one in Eq. (15), are absorbed by $\mathcal{V}_c$, while subdivergences are taken care of by counterterms for the soft vertices and lower order $\mathcal{V}_c$ counterterms. The sum of unrenormalized soft-static and purely soft diagrams in the effective theory agree. So if these were the only considerations, then the description of these effects would be basically a matter of convenience. However, divergences associated with ultrasoft gluons can only be absorbed into $\mathcal{V}_c$, so at the level that these gluons contribute in the effective theory it is necessary to adopt the four quark operator description from the start (i.e. just below the scale m).

To calculate the NLL energy we also need the two-loop anomalous dimension for $\mathcal{V}_c$, which is obtained from the renormalization of order α_s^3/v diagrams. At this order there are effective theory graphs with iterations of potentials, shown in Fig. 5, and soft effective theory diagrams, as in Fig. 6. Graphs with ultrasoft gluons do not contribute at this order. The potential diagrams are finite in the ultraviolet and reproduce the Coulombic singularities in perturbative QCD. The contributions from the soft diagrams can be determined from the soft-static potential calculations. For the color singlet channel, the UV divergences in the soft-static two-loop diagrams were calculated in Ref. [20] and the constant terms in Refs. [11,12]. The sum of unrenormalized soft diagrams has the form

$$\frac{i\alpha_S^3(\nu)}{\mathbf{k^2}}\frac{C_F}{4\pi}\biggl[\frac{\beta_0^2}{\epsilon^2}+\frac{\beta_1+2\beta_0 a_1}{\epsilon}+\frac{2\beta_0^2}{\epsilon}\ln\Bigl(\frac{\mu_S^2}{\mathbf{k^2}}\Bigr)+\beta_0^2\ln^2\Bigl(\frac{\mu_S^2}{\mathbf{k^2}}\Bigr)+(\beta_1+2\beta_0 a_1)\ln\Bigl(\frac{\mu_S^2}{\mathbf{k^2}}\Bigr)+a_2^{(a)}\biggr]. \quad (17)$$

The effective theory counterterm graphs give

$$-\frac{i\alpha_S^3(\nu)}{\mathbf{k^2}}\frac{C_F}{4\pi}\biggl[\frac{2\beta_0^2}{\epsilon^2}+\frac{2\beta_0^2}{\epsilon}\ln\Bigl(\frac{\mu_S^2}{\mathbf{k^2}}\Bigr)+\frac{2a_1\beta_0}{\epsilon}+a_2^{(b)}\biggr]. \quad (18)$$

Taking the sum of Eqs. (17) and (18) we find that up to two-loops the counterterm for the color singlet Coulomb potential has the form

$$Z_c = 1 - \frac{\alpha_S(\nu)\beta_0}{4\pi\epsilon} + \frac{\alpha_S^2(\nu)}{(4\pi)^2}\left[\frac{\beta_0^2}{\epsilon^2} - \frac{\beta_1}{\epsilon}\right], \tag{19}$$

where $\beta_1 = 34C_A^2/3 - 4C_F T_F n_\ell - 20C_A T_F n_\ell/3$. The α_s^2/ϵ divergence is proportional to β_1, so the two-loop anomalous dimension for $\mathcal{V}_c^{(s)}$ is determined by the two-loop $\overline{\rm MS}$ β-function, and the NLL coefficient of the singlet Coulomb potential is $\mathcal{V}_c^{(s)}(\nu) = 4\pi\overline{\alpha}_s^{[2]}(m\nu)$.

The energy at NLL order involves including the NLL coefficient for the Coulomb potential, $\mathcal{V}_c^{(s)}(\nu)$ in Eq. (14a), and calculating the matrix element of the one-loop order $1/v$ soft diagram between Coulombic states [$a_c(\nu) \equiv -\mathcal{V}_c^{(s)}(\nu)/4\pi$]

$$i\left\langle \quad \right\rangle = -C_F\,\alpha_S^2(\nu)\left\langle \frac{1}{\mathbf{k^2}}\left[a_1 + \beta_0 \ln\left(\frac{\mu_S^2}{\mathbf{k^2}}\right)\right]\right\rangle \tag{20}$$

$$= -\frac{m\,C_F\,\alpha_S^2(\nu)a_c(\nu)}{8\pi\,n^2}\left\{a_1 + 2\beta_0\left[\ln\left(\frac{n\,\nu}{a_c(\nu)}\right) + \psi(n+l+1) + \gamma_E\right]\right\}.$$

As expected, at the low scale $\nu \simeq v_b$, there are no large logarithms in the matrix element. Combining Eq. (20) with Eq. (14a) gives the energy valid at NLL order,

$$\Delta E^{LL} + \Delta E^{NLL} = -\frac{m}{4n^2}\left[a_c(v_b)\right]^2 - \frac{m\,C_F\,\alpha_S^2(v_b)a_c(v_b)}{8\pi\,n^2}\left\{2\beta_0\Big[\psi(n+l+1) + \gamma_E\Big] + a_1\right\}. \tag{21}$$

In the next section, the three-loop running of the Coulomb potential will be derived. We therefore need the two loop matching condition, and so consider the finite parts for the two loop graphs. The sum of renormalized soft diagrams in Fig. 6 is

$$\frac{i\alpha_S^3(\nu)}{\mathbf{k^2}}\frac{C_F}{4\pi}\left[\beta_0^2\ln^2\left(\frac{\mu_S^2}{\mathbf{k^2}}\right) + (\beta_1 + 2\beta_0 a_1)\ln\left(\frac{\mu_S^2}{\mathbf{k^2}}\right) + a_2\right], \tag{22}$$

where from Ref. [12] the sum of constants in Eqs. (17) and (18) is $a_2 = a_2^{(a)} + a_2^{(b)} = 456.75 - 66.354 n_\ell + 1.235 n_\ell^2$ for n_ℓ light flavors. The matching coefficient for $\mathcal{V}_c$ at the scale m is given by the difference between the $1/\mathbf{k}^2$ terms in the $Q\bar{Q}$ scattering amplitude in the full and effective theories. It is convenient to analyze the two loop result in the full theory by using regions in the threshold expansion [21]. The soft region exactly reproduces the result from the soft graphs. Furthermore, the potential region exactly reproduces the results for the potential graphs in Fig. 5. Thus, the matching correction for $\mathcal{V}_c(1)$ is also zero at two-loops. In general, a non-zero matching correction appears when there is a full theory contribution from an off-shell region such as the hard regime or when UV divergences appear

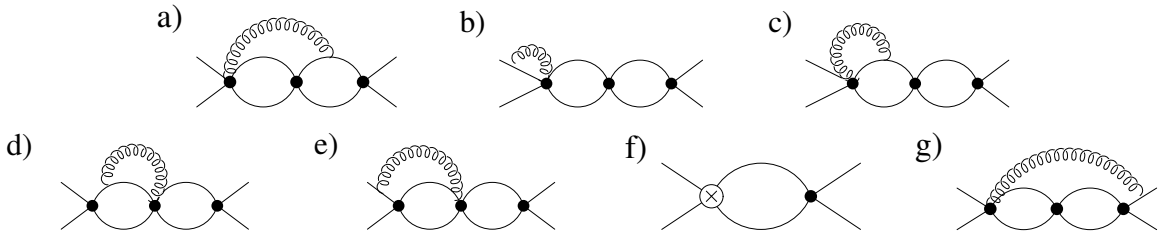

FIG. 7. Graphs with ultrasoft gluons which do not contribute to the running of the Coulomb potential. The divergences in a)-e) are canceled by graph f) which has an insertion of the corresponding $\mathcal{V}_k$ counterterm(s) denoted by $\otimes$. Graph g) is UV finite.

in the effective theory graphs.[3] In the full theory at two loops there are no contributions proportional to $1/\mathbf{k}^2$ from off-shell regions. The soft effective theory graphs are UV divergent, however these divergences are in one-to-one correspondence with UV divergences in the full or static theory. Finally, the graphs with iterations of potentials are UV finite.

V. THREE-LOOP RUNNING OF $\mathcal{V}_c$

To compute the three-loop anomalous dimension for the Coulomb potential we need to evaluate the UV divergent graphs in the effective theory that are order α_s^4/v. We begin by considering diagrams with an ultrasoft gluon. In Coulomb gauge we have graphs with $\mathbf{p}\cdot\mathbf{A}/m$ vertices as well as the coupling of ultrasoft gluons to the Coulomb potential from the operator [6]

$$\mathcal{L} = \frac{2i\,\mathcal{V}_c^{(T)}\,f^{ABC}}{\mathbf{k}^4}\mu_S^{2\epsilon}\mu_U^{\epsilon}\,\mathbf{k}\cdot(g\mathbf{A}^C)\,\psi^\dagger_{\mathbf{p}'}\,T^A\psi_{\mathbf{p}}\,\chi^\dagger_{-\mathbf{p}'}\,\bar{T}^B\chi_{-\mathbf{p}}\,. \tag{23}$$

All graphs with two $\mathbf{p}\cdot\mathbf{A}$ vertices are UV finite or are canceled by two loop graphs with insertions of the one-loop counterterms for $\mathcal{V}_2$ and $\mathcal{V}_r$ computed in Ref. [4]. The remaining diagrams are shown in Figs. 7 and 8. Graphs 7a through 7e have UV subdivergences which are exactly canceled by the diagram with $\mathcal{V}_k$ counterterms shown in Fig. 7f. These graphs contain subdivergences that were responsible for the running of the $1/(m|\mathbf{k}|)$ potential at two-loops [6]. Graph 7g is UV finite.

The divergent diagrams with an ultrasoft gluon which are not completely canceled by a counterterm diagram are shown in Fig. 8. Consider the three-loop graph in Fig. 8a with

[3] An example where UV divergences in the effective theory affect the matching is the two-loop coefficient for the production current.

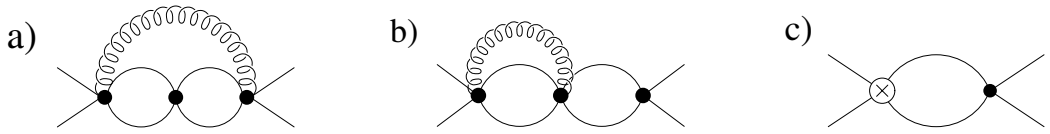

FIG. 8. Graphs with an ultrasoft gluon which contributes to the three-loop running of the Coulomb potential.

momenta l for the loop with the ultrasoft gluon and k and q for the remaining loops. After performing the k^0 and q^0 integrals by contours, the loop integration involving l is

$$\int d^d l \, \frac{\delta^{ij} - \mathbf{l^i l^j}/\mathbf{l^2}}{l^2(l^0 + E - \mathbf{k^2}/m)(l^0 + E - \mathbf{q^2}/m)} \, . \tag{24}$$

From this expression we see that the ultrasoft momentum l and potential momentum, $\mathbf{k}$ and $\mathbf{q}$, are not completely separable since they appear in the same propagator. The l integration produces an UV divergence while the remaining integrations are UV and IR finite[4]. Evaluating the remaining integrals gives

$$\text{Fig. 8a} = \frac{4i}{3}(\mathcal{C}_{8a}) \frac{\left[\mathcal{V}_c^{(T)}(\nu)\right]^3 \alpha_U(\nu) \mu_S^{2\epsilon}}{(4\pi)^3 \, \mathbf{k^2}} \left[\frac{1}{\epsilon} + \ln\left(\frac{\mu_U^2}{E^2}\right) + 2\ln\left(\frac{\mu_S^2}{\mathbf{k^2}}\right) + \ldots \right], \tag{25}$$

where the color factor is

$$(\mathcal{C}_{8a}) = C_A C_1 \left[\frac{(C_A + C_d)}{8} 1 \otimes 1 + T \otimes \bar{T} \right], \tag{26}$$

and for gauge group SU(N_c), $C_d = N_c - 4/N_c$ and $C_1 = (N_c^2 - 1)/(4N_c^2)$. The graph in Fig. 8c involves the iteration of a $1/\mathbf{k^2}$ potential and a $\mathcal{V}_k$ counterterm and also has a Coulombic infrared divergence. This graph cancels the corresponding product of IR and UV divergences arising in Fig. 8b. The sum of graphs in Fig. 8b,c still has an UV divergence, and we find

$$\text{Fig. 8b} + \text{8c} = -\frac{4i}{3}(\mathcal{C}_{8bc}) \frac{\left[\mathcal{V}_c^{(T)}(\nu)\right]^3 \alpha_U(\nu) \mu_S^{2\epsilon}}{(4\pi)^3 \, \mathbf{k^2}} \left[\frac{1}{\epsilon} + \ln\left(\frac{\mu_U^2}{E^2}\right) + 2\ln\left(\frac{\mu_S^2}{\mathbf{k^2}}\right) + \ldots \right], \tag{27}$$

where the color factor is

$$(\mathcal{C}_{8bc}) = C_A \left[\frac{C_1(C_A + C_d)}{8} 1 \otimes 1 - \left(C_1 + \frac{(C_A + C_d)^2}{32} \right) T \otimes \bar{T} \right]. \tag{28}$$

The sum of divergences in Eqs. (25) and (27) are canceled by a three-loop counterterm for $\mathcal{V}_c$. Differentiating with respect to $\ln \mu_S$ and $\ln \mu_U$ gives the anomalous dimensions

---

[4]For static quarks this three-loop graph also has an IR divergence [18], but in the non-static case we find that this divergence is regulated by the quark kinetic energy.

$$\gamma_U = \frac{8}{3}\Big[2C_AC_1 + \frac{C_A(C_A+C_d)^2}{32}\Big]\frac{\Big[\mathcal{V}_c^{(T)}(\nu)\Big]^3}{(4\pi)^3}\,\alpha_U(\nu)\,\Big(T\otimes\bar{T}\Big)\,,$$
$$\gamma_S = \frac{16}{3}\Big[2C_AC_1 + \frac{C_A(C_A+C_d)^2}{32}\Big]\frac{\Big[\mathcal{V}_c^{(T)}(\nu)\Big]^3}{(4\pi)^3}\,\alpha_U(\nu)\,\Big(T\otimes\bar{T}\Big)\,. \tag{29}$$

The total anomalous dimension from the ultrasoft diagrams is $\gamma = 2\gamma_U + \gamma_S$, so

$$\gamma = \frac{32}{3}\Big[2C_AC_1 + \frac{C_A(C_A+C_d)^2}{32}\Big]\frac{\Big[\mathcal{V}_c^{(T)}(\nu)\Big]^3}{(4\pi)^3}\,\alpha_U(\nu)\,\Big(T\otimes\bar{T}\Big)\,. \tag{30}$$

The presence of an ultraviolet divergence in the ultrasoft graphs induces an additional ultraviolet divergence in the soft graphs (as discussed further in Appendix A). This divergence induces an additional contribution to the soft anomalous dimension:

$$\gamma_S = -8\Big[2C_AC_1 + \frac{C_A(C_A+C_d)^2}{32}\Big]\,\alpha_S^4(\nu)\,\Big(T\otimes\bar{T}\Big)\,. \tag{31}$$

For the Coulomb potential the remaining UV divergences in the soft graphs correspond to divergences which are canceled in the static calculation by field, vertex, and coupling renormalization. As discussed before, these divergences give a contribution proportional to the three-loop $\overline{\rm MS}$ β-function, so for the color singlet channel we have the additional contribution

$$\gamma_S^{(s)} = 2C_F\beta_2\frac{\alpha_S^4(\nu)}{(4\pi)^2}\,. \tag{32}$$

For QCD, $\beta_2 = 2857/2 - 5033n_\ell/18 + 325n_\ell^2/54$ for n_ℓ light flavors.

Combining Eqs. (30)–(32) in the color singlet channel and using the LL relation $\mathcal{V}_c^{(T)}(\nu) = 4\pi\alpha_S(\nu)$ gives the total anomalous dimension for the Coulomb potential to three-loop order

$$\begin{aligned}\gamma_{\rm total}^{(s)} = {}& 2C_F\Big[\beta_0\alpha_S^2(\nu) + \beta_1\frac{\alpha_S^3(\nu)}{4\pi} + \beta_2\frac{\alpha_S^4(\nu)}{(4\pi)^2}\Big]\\ & -C_A^3C_F\Big[\frac{4}{3}\alpha_S^3(\nu)\alpha_U(\nu) - \alpha_S^4(\nu)\Big]\,.\end{aligned} \tag{33}$$

Solving this equation with the two-loop boundary condition $\mathcal{V}_c^{(s)}(1) = -4\pi C_F\alpha_s(m)$, the NNLL result for the running Coulomb potential is

$$\mathcal{V}_c^{(s)}(\nu) = -4\pi C_F\overline{\alpha}_s^{[3]}(m\nu) + \frac{8\pi C_FC_A^3}{3\beta_0}\,\alpha_s^3(m)\,\Big[\frac{11}{4} - 2z - \frac{z^2}{2} - \frac{z^3}{4} + 4\ln(w)\Big]\,, \tag{34}$$

where

$$z = \frac{\overline{\alpha}_s^{[1]}(m\nu)}{\alpha_s(m)}\,, \qquad w = \frac{\overline{\alpha}_s^{[1]}(m\nu^2)}{\overline{\alpha}_s^{[1]}(m\nu)}\,. \tag{35}$$

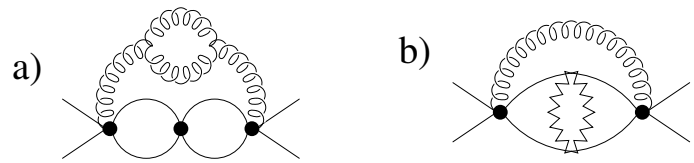

FIG. 9. Graphs with double logarithms that are determined from Fig. 8a.

To compare to the static potential result from Ref. [7] we can expand the running couplings in $\alpha_s(m)$. Ignoring the $\overline{\alpha}_s^{[3]}(m\nu)$ term, the remaining logarithms in the $\mathcal{V}_c^{(s)}(\nu)$ coefficient are

$$-\frac{1}{3}\,C_F C_A^3\,\alpha_s^4(m)\ln(\nu) + \frac{2\beta_0}{3\pi}\,C_F C_A^3\,\alpha_s^5(m)\ln^2(\nu) - \frac{17\beta_0^2}{18\pi^2}\,C_F C_A^3\,\alpha_s^6(m)\ln^3(\nu) + \ldots\,. \qquad (36)$$

Expanding the analogous contribution to the static result in Eq. (7) from Ref. [7], taking $\mu = m\nu^2$ and $r = 1/m\nu$, gives

$$-\frac{1}{3}\,C_F C_A^3\,\alpha_s^4(m)\ln(\nu) + \frac{3\beta_0}{4\pi}\,C_F C_A^3\,\alpha_s^5(m)\ln^2(\nu) - \frac{77\beta_0^2}{72\pi^2}\,C_F C_A^3\,\alpha_s^6(m)\ln^3(\nu) + \ldots\,. \qquad (37)$$

From Eqs. (36) and (37) we see that the single $\ln(\nu)$ terms agree, but the higher order logarithms differ.

The origin of the difference between the running of the Coulomb and static potentials is the relation between scales for the case of moving versus fixed quarks. For the Coulomb potential the non-relativistic quarks obey the dispersion relation $E = \mathbf{p}^2/(2m)$, which relates the energy and momentum scales, and logarithms of E, $\mathbf{p}$ and $\mathbf{k}$ cannot be treated independently. The anomalous dimension in Eq. (33) generates $\ln^2(\nu)$ terms that reproduce the double logarithms that appear when diagrams such as the ones in Fig. 9 are evaluated at the hard scale m. The graph in Fig. 9a includes a vacuum polarization loop for the ultrasoft gluon which only sees the scale mv^2, while the soft loop in Fig. 9b sees only the scale mv. Even though each of the two logarithms in Fig. 9b comes from a different ratio of low energy scales, the modes in the graph must be included at the same time since in the effective theory the division between soft and ultrasoft modes (and the multipole expansion) occur right at the scale m. Furthermore, for all scales below m the couplings for soft and ultrasoft gluons run at different rates. As mentioned in the introduction, this correlation of E, $\mathbf{p}$ and the momentum transfer $\mathbf{k}$ has been tested successfully for bound states in QED [8].

In contrast, consider the situation with two static quarks where the distance between them, $r \sim 1/|\mathbf{k}|$, is held fixed externally, and the energy fluctuations are about $E = 0$. In this case the scales r and E are not correlated. Furthermore, operators with powers of $1/m$

play no role in the calculation of the anomalous dimension, unlike the Coulombic case with an expansion in the velocity. The difference between the static and non-static calculations occurs essentially because neither the $m \to \infty$ nor the $v \to 0$ limit of the effective theory is the same as the static theory.

VI. THE NNLL ENERGY FOR A $Q\overline{Q}$ BOUND STATE

The energy at NNLL has contributions from matrix elements of operators of order

$$\left\{\frac{\alpha_s^4}{v^2},\ \frac{\alpha_s^3}{v},\ \alpha_s^2 v^0,\ \alpha_s v,\ v^2\right\} .$$

There are contributions from tree level matrix elements, which include the $\mathbf{p^4}/m^3$ operator ($\sim v^2$), the order v potentials with LL coefficients ($\sim \alpha_s v$), the order v^0 potentials with NLL coefficients ($\sim \alpha_s^2 v^0$), and the correction to the energy from the Coulomb potential with the NNLL coefficient ($\sim \alpha_s^3/v$). We also have the matrix element of the order α_s^3/v one loop and two loop soft diagrams in Fig. 6. Finally, there are the double insertions of two α_s^2/v soft diagrams ($\sim \alpha_s^4/v^2$). For simplicity all n_ℓ light quarks are taken to be massless.

The contributions from tree level matrix elements are [$a_c(\nu) = -\mathcal{V}_c^{(s)}(\nu)/4\pi$]

$$\left\langle V^{(0)}\right\rangle = \frac{m}{4n^3(2l+1)}\,[a_c(\nu)]^2\,\mathcal{V}_k^{(s)}(\nu)\,, \tag{38}$$

$$\begin{aligned}\left\langle V^{(1)}\right\rangle = \frac{m}{4n^3}[a_c(\nu)]^3\Bigg\{&\frac{\delta_{l0}}{2\pi}\left[\mathcal{V}_2^{(s)}(\nu) + s(s+1)\mathcal{V}_s^{(s)}(\nu)\right] - \frac{(2l+1-4n)}{8\pi n(2l+1)}\,\mathcal{V}_r^{(s)}(\nu)\\ &+ \frac{X_{ljs}\,\delta_{s1}\,(1-\delta_{l0})}{4\pi l(l+1)(2l+1)}\,\mathcal{V}_\Lambda^{(s)}(\nu) + \frac{3\langle S_{12}\rangle_{ljs}\,\delta_{s1}\,(1-\delta_{l0})}{4\pi l(l+1)(2l+1)}\,\mathcal{V}_t^{(s)}(\nu)\Bigg\},\end{aligned}$$

$$\left\langle \frac{-\mathbf{p^4}}{4m^3}\right\rangle = \frac{m}{16n^3}\,[a_c(\nu)]^4\left[\frac{3}{4n} - \frac{2}{2l+1}\right],$$

where the Wilson coefficients $\mathcal{V}_{c,k,2,s,r,\Lambda,t}^{(s)}$ are defined in section II. The matrix elements of the soft loops are

$$\begin{aligned}\left\langle i\ \raisebox{-0.5ex}{\includegraphics[height=2.2ex]{fig_soft_loop.pdf}}\ + \ldots\right\rangle = -\frac{mC_F\alpha_S^3(\nu)\,a_c(\nu)}{8\pi^2 n^2}\Bigg\{&\left(\frac{\beta_1}{2}+\beta_0 a_1\right)\left(\ln\left(\frac{n\,\nu}{a_c(\nu)}\right) + \Psi(n+l+1) + \gamma_E\right)\\ &+\frac{a_2}{4} + \beta_0^2\left(\ln^2\left(\frac{n\,\nu}{a_c(\nu)}\right) + 2\ln\left(\frac{n\,\nu}{a_c(\nu)}\right)\Big[\Psi(n+l+1)+\gamma_E\Big] + N_2(n,l)\right)\Bigg\},\end{aligned} \tag{39}$$

$$\begin{aligned}\left\langle T\Big\{i\ \raisebox{-0.5ex}{\includegraphics[height=2.2ex]{fig_soft_loop.pdf}}\ ,\ i\ \raisebox{-0.5ex}{\includegraphics[height=2.2ex]{fig_soft_loop.pdf}}\ \Big\}\right\rangle = -\frac{mC_F^2\alpha_S^4(\nu)}{16\pi^2 n^2}\Bigg\{&\frac{a_1^2}{4} + \beta_0 a_1\left(\ln\left(\frac{n\,\nu}{a_c(\nu)}\right) + 2N_1(n,l) + \gamma_E\right)\\ &+\beta_0^2\left(\ln^2\left(\frac{n\,\nu}{a_c(\nu)}\right) + 4\ln\left(\frac{n\,\nu}{a_c(\nu)}\right)\Big[N_1(n,l)+\frac{\gamma_E}{2}\Big] + 4N_0(n,l) + 4\gamma_E N_1(n,l) + \gamma_E^2\right)\Bigg\},\end{aligned}$$

where the functions $N_{0,1,2}(n,l)$, $\langle S_{12}\rangle_{ljs}$ and X_{ljs} are obtained from Refs. [22,23] and are summarized in Appendix B. The only additional contribution is the result for the NLL energy in Eq. (21) with the Wilson coefficients evaluated at one higher order.

Again, at the scale $\nu = v_b$ there are no large logarithms in the matrix elements; the large logarithms are summed up into the Wilson coefficients. For $\nu = v_b$ the energy at NNLL order in terms of the pole mass m reads

$$
\begin{aligned}
\Delta E &= \Delta E^{LL} + \Delta E^{NLL} + \Delta E^{NNLL} \qquad (40)\\
&= -\frac{m}{4n^2}\,[a_c(v_b)]^2 - \frac{m\,C_F\,\alpha_S^2(v_b) a_c(v_b)}{(8\pi\,n^2)}\Big[\,2\beta_0\Big(\psi(n+l+1)+\gamma_E\Big)+a_1\,\Big]\\
&+ \frac{m}{4n^3(2l+1)}\,[a_c(v_b)]^2\;\mathcal{V}_k^{(s)}(v_b) + \frac{m}{16n^3}\,[a_c(v_b)]^4\left[\frac{3}{4n}-\frac{2}{2l+1}\right]\\
&+ \frac{m}{4n^3}[a_c(v_b)]^3\Bigg\{\frac{\delta_{l0}}{2\pi}\left[\mathcal{V}_2^{(s)}(v_b)+s(s+1)\mathcal{V}_s^{(s)}(v_b)\right] - \frac{(2l+1-4n)}{8\pi n(2l+1)}\,\mathcal{V}_r^{(s)}(v_b)\\
&\quad + \frac{X_{ljs}\delta_{s1}(1-\delta_{l0})}{4\pi l(l+1)(2l+1)}\,\mathcal{V}_\Lambda^{(s)}(v_b) + \frac{3\langle S_{12}\rangle_{ljs}\delta_{s1}(1-\delta_{l0})}{4\pi l(l+1)(2l+1)}\,\mathcal{V}_t^{(s)}(v_b)\Bigg\}\\
&- \frac{m\,C_F\,\alpha_S^3(v_b)\,a_c(v_b)}{8\pi^2 n^2}\left\{\beta_0^2\,N_2(n,l) + \left(\frac{\beta_1}{2}+\beta_0 a_1\right)\Big[\Psi(n+l+1)+\gamma_E\Big] + \frac{a_2}{4}\right\}\\
&- \frac{mC_F^2\alpha_S^4(v_b)}{16\pi^2 n^2}\left\{\beta_0^2\Big[4N_0(n,l)+4\gamma_E N_1(n,l)+\gamma_E^2\Big] + \beta_0 a_1\Big[2N_1(n,l)+\gamma_E\Big] + \frac{a_1^2}{4}\right\}.
\end{aligned}
$$

When this expression is expanded in powers of α_s at a given renormalization scale the LL, NLL, and NNLL predictions for the energy become series in $(\alpha_s \ln \alpha_s)$ as in Eq. (3). The terms beyond NNLO that are determined unambiguously are those up to $m\alpha_s^4(\alpha_s\ln\alpha_s)^k$, $k \geq 1$. From Eq. (40) we see that up to NLL the series are determined by the running of $\overline{\alpha}_s(\mu)$ since up to NLL order we have $a_c(\nu)/C_F = \alpha_S(\nu) = \overline{\alpha}_s(m\nu)$. At NNLL order the series is no longer just determined by the QCD β-function since operators besides the strong coupling have non-trivial anomalous dimensions.

It is well known that the convergence of predictions for ΔE in terms of the pole mass are plagued by the presence of infrared renormalons. If predictions are made in terms of a short distance mass such as the $\overline{\rm MS}$ mass the leading renormalon in the pole mass and $1/\mathbf{k}^2$ potentials cancel [24,25] and the convergence of the perturbation series is improved. A phenomenological analysis, which includes the issue of renormalon cancellation in the presence of resummed logarithms, will be carried out elsewhere.

Past finite order predictions for the $Q\bar{Q}$ energies have typically been made using the strong coupling evaluated at the soft scale mv. At LO and NLO this is the natural choice

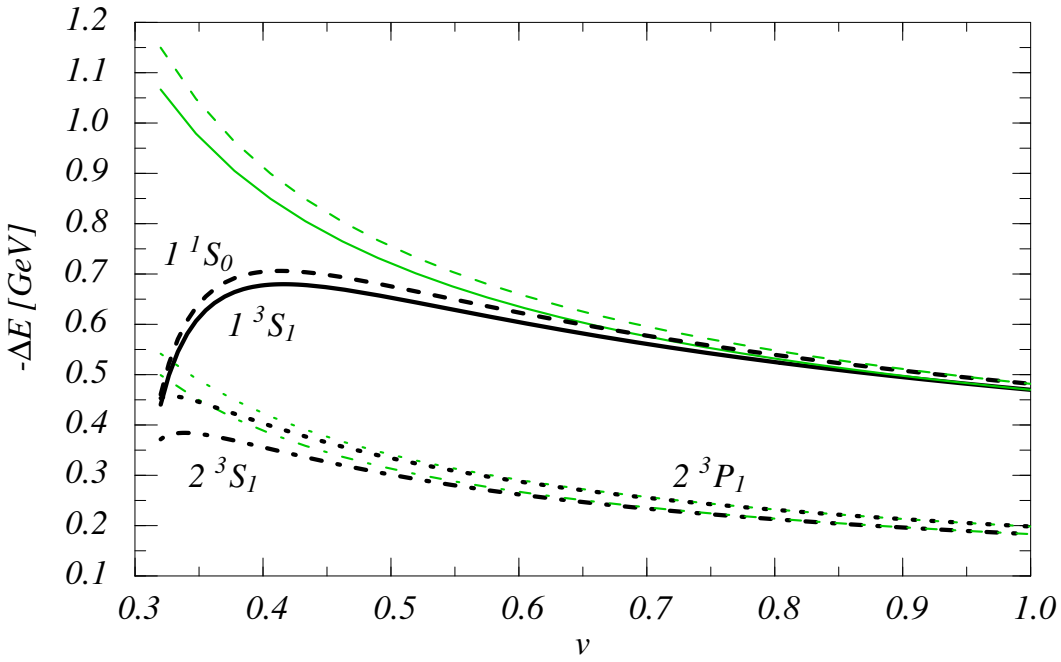

FIG. 10. Comparison of the NNLL binding energy predictions (thick black lines) with the NNLO predictions (thin green lines) for the $1\,^3S_1$ (solid), $1\,^1S_0$ (dashed), $2\,^3S_1$ (dot-dashed), and $2\,^3P_1$ (dotted) states, and for different values of the subtraction velocity ν.

since all logarithms $\alpha_s^2(\alpha_s \ln \mu)^k$ and $\alpha_s^3(\alpha_s \ln \mu)^k$ in higher order matrix elements are minimized at $\mu = |\mathbf{k}|$. Effectively this choice turns the LO and NLO results into the LL and NLL predictions. However, at NNLO this choice of μ may not be optimal since matrix elements begin to involve factors of $\alpha_s^4[\alpha_s \ln(\mu/E)]$. The NNLL prediction is not generated by a simple replacement rule and instead involves the non-trivial Wilson coefficients $\mathcal{V}_{c,k,2,s,r,\Lambda,t}(\nu)$.

In Fig. 10 we compare the NNLL energy predictions at subtraction velocity ν (thick black lines) with the NNLO predictions with coupling $\overline{\alpha}_s(m\nu)$ (thin green lines), to illustrate the impact of summing the logarithms. The displayed states include $n\,^{2S+1}L_J = 1\,^3S_1$ (solid lines), $1\,^1S_0$ (dashed lines), $2\,^3S_1$ (dash-dotted lines), and $2\,^3P_1$ (dotted lines). As input we have chosen $m_b = 4.8$ GeV for the bottom quark pole mass, $\alpha_s^{(n_\ell=4)}(m_b) = 0.22$, and have included three-loop running for the evolution of the strong coupling to lower scales. The NNLO and the NNLL energies are equal for $\nu = 1$, because no logarithms are summed into the Wilson coefficients. The summation has the largest impact on the $n = 1$ S-wave states, and in all cases reduces the size of the binding energy. In Table I we summarize for ν of order a typical quark velocity, $\nu = (0.35, 0.4)$, values for the NNLO result and the renormalization group improved NNLL calculation. Relative to the NNLO results the scale uncertainty in

$b\bar{b}$ state $(n^{2S+1}L_J)$		1^1S_0	1^3S_1	2^3S_1	2^3P_1
ΔE at NNLO (MeV)	$\nu = 0.35$	-1040	-972	-449	-488
	$\nu = 0.4$	-912	-860	-389	-423
ΔE at NNLL (MeV)	$\nu = 0.35$	-641	-614	-382	-446
	$\nu = 0.4$	-705	-678	-356	-403

TABLE I. Comparison of the NNLO and NNLL predictions for the binding energy corrections (in MeV) for $b\bar{b}$ states. The NNLL results include the summation of logarithms not accounted for by $\overline{\alpha}_s(m\nu)$. Results are shown for two values of ν of order the heavy quark velocity.

the NNLL predictions is somewhat reduced.

The summation of NNLL logarithms also reduces the size of the ground state hyperfine splitting, but increases the size of the analog of the QED Lamb shift, (the $2^3S_1 - 2^3P_1$ splitting). For $\nu = (0.35, 0.4)$ and at NNLO the hyperfine splitting and the $2^3S_1 - 2^3P_1$ splitting are

$$E(1^3S_1) - E(1^1S_0) = (68, 52)\ \text{MeV}\,, \qquad E(2^3S_1) - E(2^3P_1) = (39, 35)\ \text{MeV}\,, \tag{41}$$

while at NNLL order we find

$$E(1^3S_1) - E(1^1S_0) = (27, 27)\ \text{MeV}\,, \qquad E(2^3S_1) - E(2^3P_1) = (64, 47)\ \text{MeV}\,. \tag{42}$$

Summing the logarithms reduces the perturbative contribution to the hyperfine splitting by a factor of two. The $2^3S_1 - 2^3P_1$ splitting is fairly sensitive to the value of ν.

In order to examine the size of the logarithmic terms that are summed at NNLL order we can expand Eq. (40) in powers of α_s. To suppress logarithms proportional to the QCD β-function in the energy at NNLO is it convenient to expand in the coupling $a_s \equiv \overline{\alpha}_s(mv_b)$:

$$\begin{aligned}
\Delta E = &- m\,a_s^2\Big[\,\ldots\,\Big] - m\,a_s^3\Big[\,\ldots\,\Big] - m\,a_s^4\Big[\,\ldots\,\Big] \\
&- m\,a_s^5\,\ln a_s\,\frac{C_F^2}{4\,\pi\,n^2}\Bigg\{\frac{C_A}{3}\left[\frac{C_A^2}{2} + \frac{4\,C_A\,C_F}{n\,(2l+1)} + \frac{2\,C_F^2}{n}\left(\frac{8}{2l+1} - \frac{1}{n}\right)\right] \\
&\quad + \frac{3\,\delta_{l0}\,C_F^2}{2\,n}(C_A + 2C_F) - \frac{7\,C_A\,C_F^2\,\delta_{l0}\,\delta_{s1}}{3\,n} - \frac{C_A\,C_F^2\,(1-\delta_{l0})\,\delta_{s1}}{4\,n\,l\,(l+1)\,(2l+1)}\left(4\,X_{ljs} + \langle S_{12}\rangle_{ljs}\right)\Bigg\} \\
&- m\,a_s^6\,\ln^2 a_s\,\frac{C_F^2}{4\,\pi^2\,n^2}\Bigg\{\frac{\delta_{l0}\,C_F^2}{6\,n}\left[\beta_0\left(\frac{13\,C_A}{2} - C_F\right) + \frac{C_A}{3}\left(25\,C_A + 22\,C_F\right)\right]
\end{aligned} \tag{43}$$

$$
\begin{aligned}
&-\frac{C_A\,C_F^2\,\delta_{l0}\,\delta_{s1}}{6\,n}\,\Big[\,5\,\beta_0+7\,C_A\,\Big]\\
&-\frac{C_A\,C_F^2\,(1-\delta_{l0})\,\delta_{s1}}{8\,n\,l\,(l+1)\,(2l+1)}\,\Big[\,\beta_0\,\Big(\,2\,X_{ljs}+\frac{1}{2}\,\langle S_{12}\rangle_{ljs}\,\Big)+C_A\,\Big(\,2\,X_{ljs}+\langle S_{12}\rangle_{ljs}\,\Big)\,\Big]\,\Big\}\\
&+\ldots\,.
\end{aligned}
$$

The a_s^2, a_s^3, a_s^4 terms are not displayed, but agree with the result in Ref. [23]. The terms proportional to $m\alpha_s^5\ln\alpha_s$ agree with Ref. [26]. The $m\alpha_s^6\ln^2\alpha_s$ result is new, as are higher terms in the series. Numerically we find

$$
\begin{aligned}
\frac{\Delta E(1^1S_0)}{m} &= -0.444\,a_s^2-1.595\,a_s^3-9.73\,a_s^4-8.56\,a_s^5\ln a_s-3.41\,a_s^6\ln^2 a_s-15.5\,a_s^7\ln^3 a_s\\
&\quad+\ldots\,,\\
\frac{\Delta E(1^3S_1)}{m} &= -0.444\,a_s^2-1.595\,a_s^3-8.68\,a_s^4-6.80\,a_s^5\ln a_s-0.904\,a_s^6\ln^2 a_s-12.1\,a_s^7\ln^3 a_s\\
&\quad+\ldots\,,\\
\frac{\Delta E(2^3S_1)}{m} &= -0.111\,a_s^2-0.546\,a_s^3-3.07\,a_s^4-0.961\,a_s^5\ln a_s-0.113\,a_s^6\ln^2 a_s-1.73\,a_s^7\ln^3 a_s\\
&\quad+\ldots\,,\\
\frac{\Delta E(2^3P_1)}{m} &= -0.111\,a_s^2-0.644\,a_s^3-3.22\,a_s^4-0.398\,a_s^5\ln a_s-0.005\,a_s^6\ln^2 a_s-0.752\,a_s^7\ln^3 a_s\\
&\quad+\ldots\,.
\end{aligned}
\tag{44}
$$

We note that for $(1^1S_0, 1^3S_1, 2^3S_1, 2^3P_1)$ using $a_s = 0.35$, the $a_s^5\ln a_s$ terms in Eq. (44) give $(93\%, 85\%, 84\%, 80\%)$ of the complete sum of logarithmic terms.

VII. CONCLUSION

The three-loop anomalous dimension for the Coulomb potential was computed in the presence of non-static quarks. In terms of the subtraction velocity ν the anomalous dimension depends on both $\alpha_s(m\nu)$ and $\alpha_s(m\nu^2)$. Our result differs from the three-loop anomalous dimension for the potential for static quarks. This is due to the fact that the energy and momentum scales are coupled for non-static quarks.

The perturbative energies for $Q\bar{Q}$ bound states were computed at NNLL order, including all terms of order $m\alpha_s^4(\alpha_s\ln\alpha_s)^k$, $k\geq 0$. The main effect of summing the logarithms is to reduce the binding energy for the 1^1S_0 and 1^3S_1 states by an amount of order a few hundred MeV. The effect on states with $n\geq 2$ is substantially smaller.

ACKNOWLEDGMENT

We would like to thank A. Pineda and J. Soto for discussions, and C. Bauer for comments on the manuscript. AM and IS are supported in part by the U.S. Department of Energy under contract DOE-FG03-97ER40546, and IS is also supported in part by NSERC of Canada.

APPENDIX A: ULTRAVIOLET AND INFRARED DIVERGENCES

In this appendix we discuss the structure of UV and IR divergences in the effective theory and their relation to the renormalization group running. In particular we explain why it is correct to treat all $1/\epsilon$ poles in soft gluon loops as UV divergences. This result follows from the fact that we have taken the full propagating gluon field and split it into two parts (soft and ultrasoft) which fluctuate on different length scales (mv and mv^2) and have different Feynman rules. The information that the two gluons came from a single field is reflected by a relation between the IR divergences in soft gluon diagrams and the UV divergences in the ultrasoft diagrams. Here we address how this correlation is accounted for in the presence of the relation $\mu_U = \mu_S^2/m$ between ultrasoft and soft subtraction scales.

For simplicity only diagrams with single $1/\epsilon$ poles and either purely soft or ultrasoft gluons will be discussed. Also, real Coulombic IR divergences will be dropped. A general diagram with a divergent soft gluon loop then gives a soft amplitude with the divergence structure:

$$i\mathcal{A}^S = \frac{A}{\epsilon_{UV}} + \frac{B}{\epsilon_{IR}} + C\left(\frac{1}{\epsilon_{UV}} - \frac{1}{\epsilon_{IR}}\right) = \frac{A+B}{\epsilon_{UV}} + (C-B)\left(\frac{1}{\epsilon_{UV}} - \frac{1}{\epsilon_{IR}}\right). \tag{A1}$$

Strictly speaking pure dimensional regularization does not distinguish between UV and IR divergences; however a distinction can always be made either by examining the analytic structure before expanding about $\epsilon = 0$ or by also performing the calculation with a different IR regulator. The notation in Eq. (A1) is slightly redundant so that C represents diagrams involving scaleless integrals (such as tadpole graphs), and A and B represent all other graphs. For example, for the Lamb shift in QED for Hydrogen only C is non-zero, while positronium also has non-zero A and B. At the same order in the power counting as Eq. (A1) there is an amplitude with a divergent ultrasoft gluon loop which has the form:

$$i\mathcal{A}^U = \frac{(C-B)}{\epsilon_{UV}} + \frac{D}{\epsilon_{IR}}. \tag{A2}$$

The nontrivial information is that the $(C-B)$ term in Eq. (A2) is determined by the IR divergence in the soft amplitude in Eq. (A1). In general D is independent of $C-B$ since ultrasoft graphs are not always proportional to $1/\epsilon_{UV}-1/\epsilon_{IR}$. The infrared divergence in Eq. (A2) will match with an infrared divergence in full QCD.

The renormalization group running is determined by the UV divergences. Naively, in Eq. (A1) the ϵ_{UV}'s correspond to the scale m and the ϵ_{IR}'s correspond to the scale mv, while in Eq. (A2) the ϵ_{UV}'s correspond to the scale mv and the ϵ_{IR}'s correspond to scales of order mv^2. However, examining $i\mathcal{A}^S + i\mathcal{A}^U$ we see that the $(C-B)$ term in the soft amplitude simply pulls up or transports the $1/\epsilon_{UV}$ in the ultrasoft graph to the hard scale [5]. The scale dependence of the coefficient $C-B$ in Eq. (A2) does not affect this argument since the scale dependence of $C-B$ in Eq. (A1) can be chosen arbitrary. Note that the $1/\epsilon_{IR}$ divergences in soft diagrams do not always correspond to IR divergences in QCD, which is further evidence of their unphysical nature. This is the case if $D \neq B-C$ such as for the two loop graphs contributing to the running of $\mathcal{V}_k(\nu)$ [6]. Finally, we see that setting $\epsilon_{IR}=\epsilon_{UV}$ in the soft amplitude in Eq. (A1) and running the ultrasoft modes from m to mv^2 with an anomalous dimension proportional to $C-B$ and running the soft modes from m to mv with an anomalous dimension proportional to $A+B$ correctly performs the running between the scales. This is the method used here and in Refs. [4,8].

The correspondence in Eqs. (A1) and (A2) also provides a useful calculational tool: if the UV divergences $A+C$ in the soft diagrams are known, and the combination $B-C$ is determined from the UV divergences in the ultrasoft calculation, one arrives at $(A+C)+(B-C)=A+B$ which is the combination needed to determine the soft anomalous dimension from $\mathcal{A}^S$.

APPENDIX B: FUNCTIONS THAT APPEAR IN $\Delta E^{\rm NNLL}$

The following functions of the principal and orbital quantum numbers (n,l,j) were derived in Refs. [22,23] and appear in our result in Eq. (40):

---

[5] This addition might seem strange since it involves canceling an UV and IR pole. However, for a multiscale problem what is ultraviolet and what is infrared is always relative; if we label the ϵ's by the corresponding scale then the cancellation is just $1/\epsilon(mv)-1/\epsilon(mv)=0$.

$$N_0(n,l) = \frac{\Psi(n+l+1)}{4}\Big[\Psi(n+l+1)-2\Big] + \frac{n\Gamma(n-l)}{2\Gamma(n+l+1)}\sum_{j=0}^{n-l-2}\frac{\Gamma(j+2l+2)}{\Gamma(j+1)(j+l+1-n)^3}$$
$$+\frac{n\Gamma(n+l+1)}{2\Gamma(n-l)}\sum_{j=n-l}^{\infty}\frac{\Gamma(j+1)}{\Gamma(j+2l+2)(j+l+1-n)^3}\,, \tag{B1}$$

$$N_1(n,l) = \frac{\Psi(n+l+1)}{2} - \frac{1}{2}\,, \tag{B2}$$

$$N_2(n,l) = \Big[\Psi(n+l+1)+\gamma_E\Big]^2 + \Psi'(n+l+1) + \frac{\pi^2}{12}$$
$$+\frac{2\Gamma(n-l)}{\Gamma(n+l+1)}\sum_{j=0}^{n-l-2}\frac{\Gamma(2l+2+j)}{\Gamma(j+1)(j+l+1-n)^2}\,, \tag{B3}$$

$$\langle S_{12}\rangle_{ljs} = \begin{cases} \dfrac{2(l+1)}{1-2l} & : \quad j = l-1 \\ 2 & : \quad j = l \\ \dfrac{-2\,l}{2l+3} & : \quad j = l+1 \end{cases}\,, \tag{B4}$$

$$X_{ljs} = \frac{1}{2}\Big(\,j(j+1) - l(l+1) - s(s+1)\,\Big)\,. \tag{B5}$$

REFERENCES

[1] W.E. Caswell and G.P. Lepage, Phys. Lett. **167B**, 437 (1986); G.T. Bodwin, E. Braaten and G.P. Lepage, Phys. Rev. **D51**, 1125 (1995), ibid. **D55**, 5853 (1997); P. Labelle, Phys. Rev. D **58**, 093013 (1998); M. Luke and A.V. Manohar, Phys. Rev. **D55**, 4129 (1997); A.V. Manohar, Phys. Rev. **D56**, 230 (1997); B. Grinstein and I.Z. Rothstein, Phys. Rev. **D57**, 78 (1998); M. Luke and M.J. Savage, Phys. Rev. **D57**, 413 (1998);

[2] A. Pineda and J. Soto, Nucl. Phys. Proc. Suppl. **64**, 428 (1998);

[3] M. Luke, A. Manohar and I. Rothstein, Phys. Rev. **D61**, 074025 (2000).

[4] A. V. Manohar and I. W. Stewart, Phys. Rev. D **62**, 014033 (2000).

[5] A.V. Manohar and I.W. Stewart, Phys. Rev. **D62**, 074015 (2000).

[6] A.V. Manohar and I.W. Stewart, Phys. Rev. **D63**, 54004 (2001).

[7] A. Pineda and J. Soto, Phys. Lett. **B495**, 323 (2000).

[8] A.V. Manohar and I.W. Stewart, Phys. Rev. Lett. **85**, 2248 (2000).

[9] A. H. Hoang, A. V. Manohar, I. W. Stewart and T. Teubner, hep-ph/0011254.

[10] A.V. Manohar, J. Soto, and I.W. Stewart, Phys. Lett. **B486**, 400 (2000).

[11] M. Peter, Phys. Rev. Lett. **78**, 602 (1997).

[12] Y. Schröder, Phys. Lett. B **447**, 321 (1999).

[13] Y. Chen, Y. Kuang and R. J. Oakes, Phys. Rev. **D52**, 264 (1995).

[14] A. V. Manohar and M. B. Wise, *Cambridge Monographs on Particle Physics, Nuclear Physics, and Cosmology, Vol. 10.*

[15] J. G. Gatheral, Phys. Lett. **B133**, 90 (1983).

[16] J. Frenkel and J. C. Taylor, Nucl. Phys. **B246**, 231 (1984).

[17] T. Appelquist, M. Dine and I. Muzinich, Phys. Lett. B **69**, 231 (1977); T. Appelquist, M. Dine and I. Muzinich, Phys. Rev. D **17**, 2074 (1978).

[18] N. Brambilla, A. Pineda, J. Soto and A. Vairo, Phys. Rev. **D60**, 091502 (1999).

[19] H.W. Griesshammer, Phys. Rev. **D58**, 094027 (1998).

[20] W. Fischler, Nucl. Phys. B **129**, 157 (1977).

[21] M. Beneke and V.A. Smirnov, Nucl. Phys. **B522**, 321 (1998).

[22] S. Titard and F.J. Yndurain, Phys. Rev. **D49**, 6007 (1994).

[23] A. Pineda and F. J. Yndurain, Phys. Rev. **D 58**, 094022 (1998); A. Pineda and F. J. Yndurain, Phys. Rev. **D 61**, 077505 (2000).

[24] A. H. Hoang, M. C. Smith, T. Stelzer and S. Willenbrock, Phys. Rev. D **59**, 114014 (1999).

[25] M. Beneke, Phys. Lett. B **434**, 115 (1998).

[26] N. Brambilla, A. Pineda, J. Soto and A. Vairo, Phys. Lett. **B470**, 215 (1999); see also B.A. Kniehl and A.A. Penin, Nucl. Phys. **B563**, 200 (1999).